PP-12

MICROWAVE CHARACTERISTICS OF GaAs MMIC INTEGRATABLE OPTICAL DETECTORS

Paul C. Claspy*, Scott M. Hill†, and Kul B. Bhasin

NASA Lewis Research Center, Cleveland, OH 44135

Abstract

Interdigitated photoconductive detectors have been fabricated on microwave device structures, making them easily integratable with MMIC's. Detector responsivity as high as 2.5 A/W and an external quantum efficiency of 3.81 were measured. Response speed was nearly independent of electrode geometry, and all detectors had usable response at frequencies to 6 GHz. A small signal model of the detectors based on microwave measurements is also developed.

Introduction

Over the past few years technology advances have occurred which have increased the possibility that in the near future phased array antennas composed of monolithic microwave integrated circuits (MMIC's) will become a practical reality.[1] To take maximum advantage of the potential size reduction that this advance represents it will be essential to effect a similar size reduction in the chip-to-chip high frequency interconnects that the system will require. Various authors have suggested that fiber optic links, which are small and lightweight, may be a viable alternative to coaxial cables and waveguides for this application.[2] If these links are to be practical, however, high frequency optical transmitters and receivers must be available, and it would be particularly desirable that optical components be process- and material-compatible with GaAs heterostructure MMIC's so that they can be integrated onto the same chip.

In this paper we report the results of a study of the optical and electrical characteristics of interdigitated photoconductive detectors of various geometries that were fabricated on a HEMT-type heterostructure material. The operating wavelength was chosen to be 820 nm.

Detector Fabrication

The detectors were fabricated on the MBE-grown GaAlAs/GaAs heterostructure material shown schematically in Fig. 1. A typical detector is shown in Fig. 2. Interdigitated electrode geometries, with finger spacings ranging from 1 to 4 μm, were used because they increase the effective active area of the detector while keeping the transit distance small. Since the GaAlAs window that remains after fabrication is essentially transparent to the incident 820 nm radiation, almost all of the photon absorption, and therefore the electron-hole pair generation, occurs within the undoped GaAs layer. For testing, the detectors were mounted directly on the Teflon insulation of a specially prepared length of semi-rigid coaxial cable, with short wire-bonded leads to the center conductor and the shield.

Optical Response Measurements

Frequency domain response measurements were made over the range 0.01 to 10 GHz using the system shown schematically in Fig. 3, and normalized responses of detectors of three different geometries are shown in Fig. 4. The detectors exhibit nearly identical response dispersion, with a 3 dB cutoff frequency at approximately 185 MHz. The gain decays at about 12 dB/decade in the decade between 100 MHz and 1 GHz, with a small plateau at 510 MHz, then falls off at 20 dB/decade after a larger plateau at 1 GHz. The shape of the response suggests that device characteristics are limited by trapping effects.[3]

Detector responsivities at 500 MHz, R(500 MHz), were measured using an Ortel SL620 diode laser, and lie in the range 0.13 to 0.31 A/W. On the basis of measurements at 500 MHz, the low frequency responsivity of the 1 by 1 μm detector was calculated to be 2.5 A/W. The (internal) quantum efficiency of this detector is 5.44, and the external quantum efficiency is 3.81, all of which are comparable to results reported for GaAs detectors.

*P.C. Claspy is a National Research Council - NASA Senior Research Associate. Permanent address: Department of Electrical Engineering and Applied Physics, Case Western Reserve University, Cleveland, Ohio 44106.

†Graduate student, Case Western Reserve University.

CH2725-0/89/0000-1163$01.00 © 1989 IEEE

Microwave Impedance Measurements and Model

DC and AC impedance characteristics of the detectors were studied under various levels of illumination. DC I-V curves for our detectors were taken using white light illumination, and a typical result is given in Fig. 5. The DC resistance of the detectors is low and constant for small bias, smoothly increases as the bias is increased, becoming very large at high bias as a result of carrier velocity saturation. The decrease of resistance with increasing optical power is also shown in Fig. 5.

The reflection coefficient, S_{11}, was measured over the frequency range 0.5 to 5.5 GHz at various bias levels and incident white light intensities using an HP-4910 Network Analyzer. Some results of these measurements are shown in Figs. 6 to 8. Figure 6 shows that S_{11} decreases with detector feature size, Fig. 7 shows that it increases with bias voltage, at moderate illumination, and Fig. 8 shows that it decreases with increasing illumination, at moderate bias.

A small-signal, high frequency model, consisting of a parallel RC combination with an inductance in series with each node of the RC network, as shown in Fig. 9(a), was developed from the measured S_{11} results. The model, which is similar to that developed by Wojtczuk and Ballantyne[4] leads to a complex impedance given by

$$Z = \frac{R(V,\Phi) + j\omega \{(L_1 + L_2) - CR^2(\omega,\Phi)\}}{1 + \omega CR^2(V,\Phi)} \qquad (1)$$

where the resistance, $R(V,\Phi)$, is a function of both the DC bias and the illumination.

The light intensity primarily affects R, which at low bias drops from well over 100 Ω at ambient to only a few tens of ohms at high intensity. Therefore, at low bias and high light level the low resistance effectively short-circuits the device capacitance, reducing the impedance to

$$Z = R + j\omega(L_1 + L_2), \qquad (2)$$

as shown in Fig. 9(b). The AC resistance was observed to increase significantly with bias, so that at high bias the complex impedance eventually simplifies to

$$Z = \frac{R}{\omega CR^2} - \frac{j}{\omega C}, \qquad (3)$$

as shown in Fig. 9(c). This change from inductive to capacitive behavior suggests the possibility of a zero reactance operating point by the elimination of any RC or R/L time constants if the detector is time constant limited. The impedance of the zero reactance point is determined by setting the imaginary part of Eq. (1) equal to zero. Then, if $(\omega CR^2) << 1$, the impedance reduces to

$$Z = \sqrt{(L_1 + L_2)/C}, \qquad (4)$$

which for our devices is about 250 Ω at somewhat less than 3 V bias.

Summary and Conclusion

The high frequency characteristics of interdigitated photoconductive detectors fabricated on a HEMT structure have been presented. The fabrication process was completely compatible with that used to fabricate MODFET's making these detectors easily integrable for MMIC usage. It should be noted that while the detectors did not exhibit an extremely high bandwidth, they did possess usable response well into the GHz range, and the change from inductive to capacitive reactance with bias suggests the possibility of a zero reactance operating point. In conclusion, then, the combination of fabrication compatibility and performance characteristics makes these devices interesting for interconnection applications.

References

1. J. Frey, and K.B. Bhasin, eds., Microwave Integrated Circuits, 2nd Ed. Dedham, MA: Artech House, 1985.

2. K.B. Bhasin, G. Anzic, R.R. Kunath, and D.J. Connolly, "Optical Techniques to Feed and Control GaAs MMIC Modules for Phased Array Antenna Applications," in AIAA 11th Annual Communications Satellite Systems Conference, New York: AIAA, pp. 506-514, 1986 (NASA TM-87218).

3. G.J. Papaionannou, and J.R. Forrest, "On the Photoresponse of GaAs MESFET's: Backgating and Deep Traps Effect," IEEE Trans. Electron Devices, vol. ED-33, no. 3, pp. 373-378, Mar. 1986.

4. S.J. Wojtczuk, and J.M. Ballantyne, "Impedance Properties and Broad-Band Operation of GaAs Photoconductive Detectors," J. Lightwave Tech., vol. LT-5, no. 3, pp. 320-324, Mar. 1987.

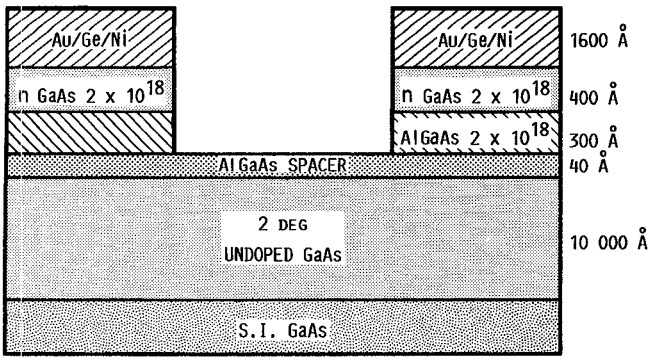

Fig. 1. Schematic cross section of photodetector material.

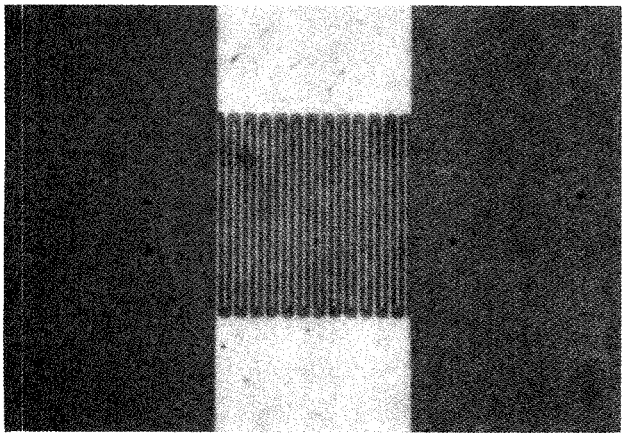

Fig. 2. 1 μm x 1 μm detector.

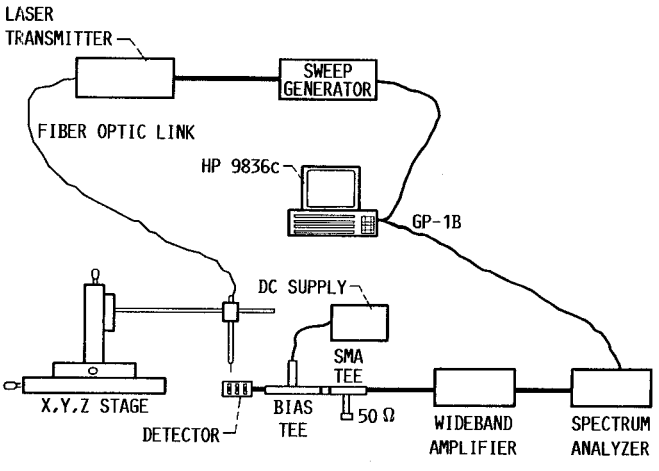

Fig. 3. Frequency domain measurement system.

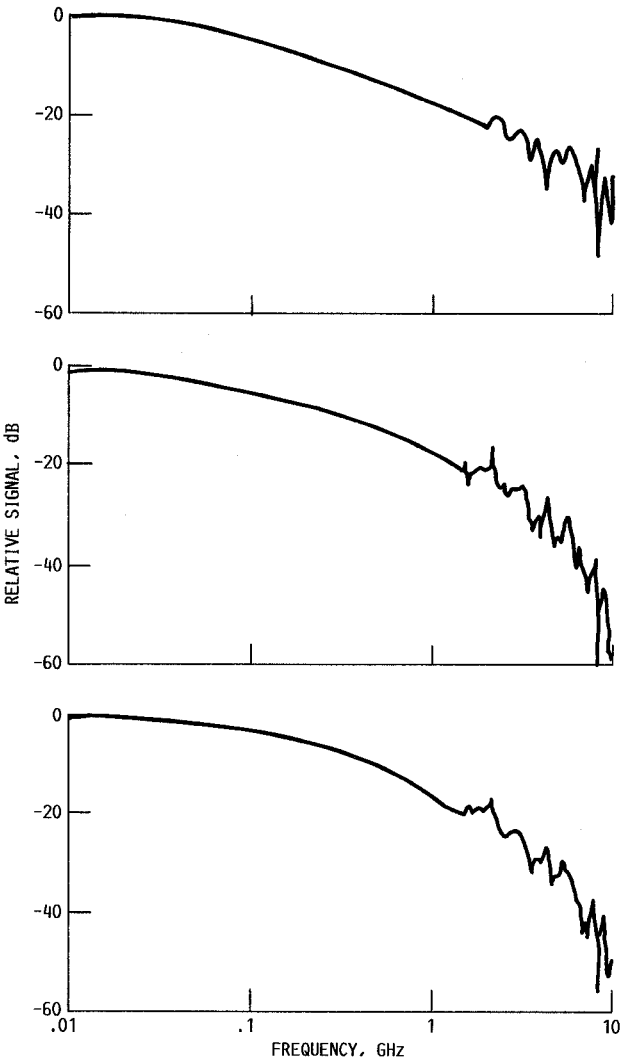

Fig. 4. Normalized frequency response of typical detectors.
(a) 1 μ x 1 μm; (b) 2 μm x 2 μm;
(c) 2 μm x 2 μm.

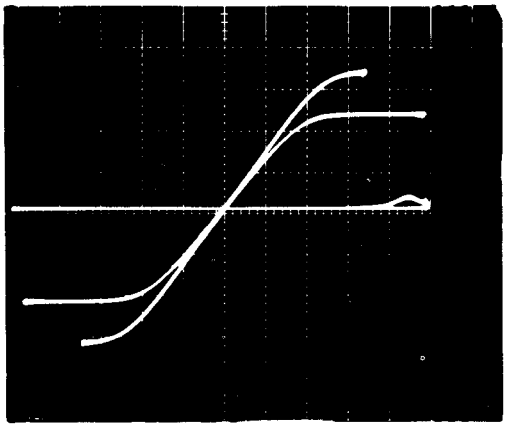

Fig. 5. I-V characteristic curve for 1 μm x 1 μm detector.

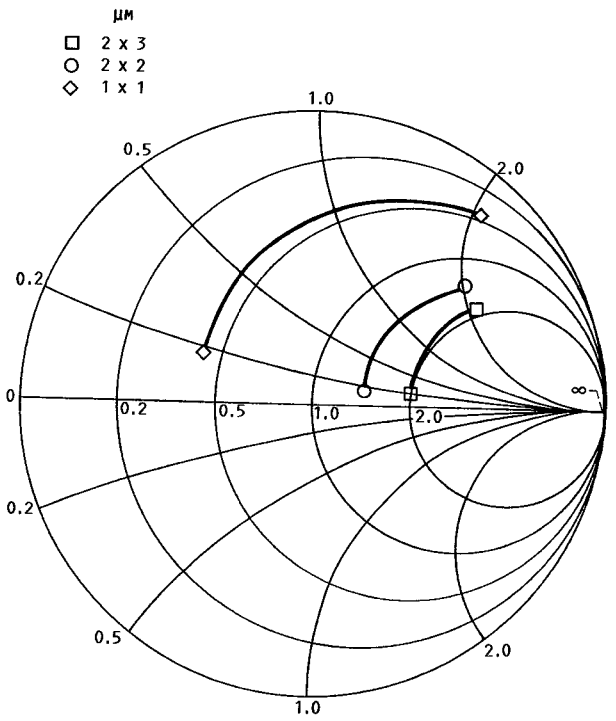

Fig. 6. Effect of electrode geometry on S_{11}.

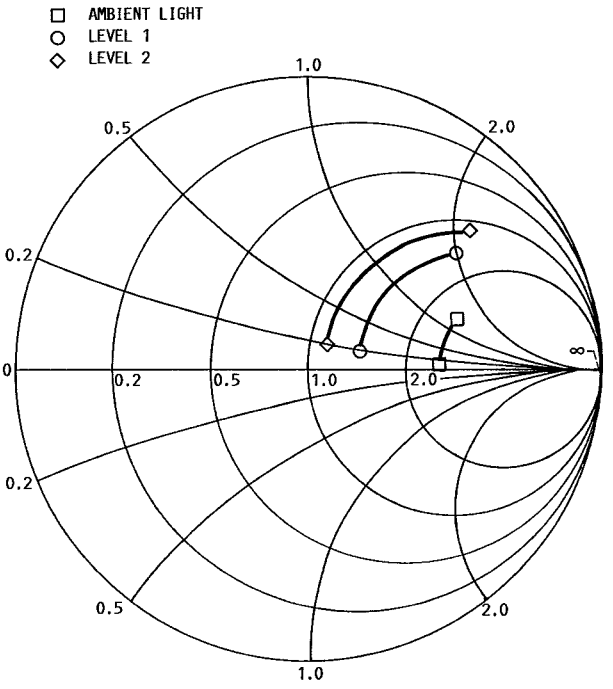

Fig. 8. Effect of illumination on S_{11} for 2 μm x 2 μm detector.

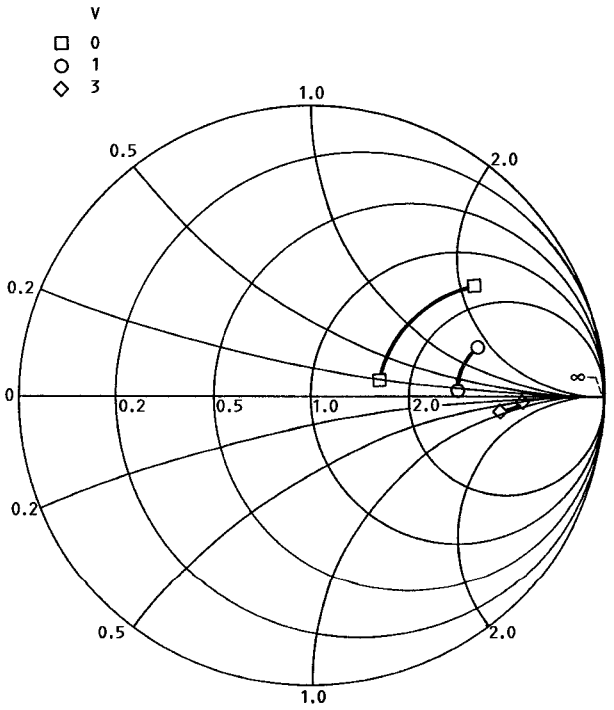

Fig. 7. Effect of bias voltage on S_{11} for 2 μm x 3 μm detector.

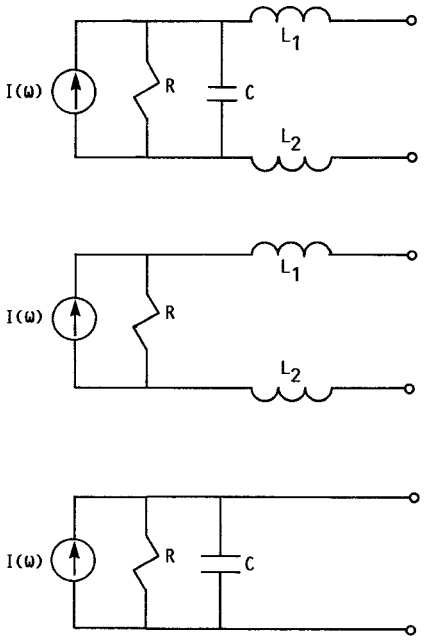

Fig. 9 Detector equivalent circuit models. (a) General equivalent circuit; (b) Low bias equivalent circuit; (c) High bias equivalent circuit.